Article

Not peer-reviewed version

Effects of the Doping of La and Ce in the $Pt/B-TiO_2$ Catalyst in Selective Oxidation Reaction of Glycerol

Zhihui Wang , Xueqiong Zhang , Bo Hai , Hao Zhang , Lijun Ding *

Posted Date: 24 February 2025

doi: 10.20944/preprints202502.1812.v1

Keywords: doping; black TiO_2; glycerol oxidation

Article

Effects of the Doping of La and Ce in the Pt/B-TiO_2 Catalyst in Selective Oxidation Reaction of Glycerol

Zhihui Wang [1], Xueqiong Zhang [1], Bo Hai [1], Hao Zhang [1] and Lijun Ding [1,2,*]

[1] College of Science Inner Mongolia Agricultural University Hohhot 010018, P. R. China
[2] Key Laboratory of the Development and Resource Utilization of Biological Pesticide in Inner Mongolia
* Correspondence: dlj78@163.com

Abstract: The increased production of biodiesel results in a corresponding rise in the production of glycerol (GLY) as a by-product. The selective oxidation of glycerol can yield relatively simple products under mild reaction conditions, offering high added value and positioning it as one of the most promising methods for industrialization. In this study, we employed black titanium dioxide (B-TiO_2) as a support and deposited platinum (Pt) to create a noble metal-supported catalyst. Lanthanum (La) or cerium (Ce) was doped into B-TiO_2 to enhance the concentration of oxygen vacancies in the support, thereby improving catalyst activity. Throughout the research process, we also investigated the impact of varying amounts of La or Ce doping on catalyst performance. Analysis of the catalytic experimental data revealed that Pt/30%Ce-B-TiO_2 exhibited the highest catalytic performance. Structural analysis of the catalysts showed that the synergistic effect between Pt0 and oxygen vacancies contributed to enhancing catalyst activity.

Keywords: doping; black TiO_2; glycerol oxidation

---

1. Introduction

In the field of modern catalytic science, the development of efficient catalysts is essential for promoting the sustainable advancement of the chemical industry. In recent years, the glycerol oxidation reaction has garnered significant attention as a crucial process for converting glycerol, a by-product of biodiesel production, into high value-added products.[1,2] Traditional catalysts often face challenges such as low conversion rates, poor selectivity, and insufficient stability during glycerol oxidation reactions, prompting researchers to continuously explore new types of catalytic materials.[3–5] Titanium dioxide (TiO_2) has gained considerable interest due to its excellent chemical and thermal stability and is commonly utilized as a support material for catalysts. However, the catalytic activity of current TiO_2-supported materials still requires enhancement.[6] As research progresses, the doping of rare earth elements into support materials has emerged as an effective strategy to improve catalytic activity, addressing the performance limitations of traditional catalysts while meeting growing industrial demands and environmental challenges. The unique electron layer structure and variable oxidation states of rare earth elements allow for the introduction of new active sites and electron transfer pathways into various catalytic materials, thereby significantly enhancing catalyst performance.[7–9] In thermal catalytic reactions, the advantages of doping with rare earth elements are particularly pronounced. For instance, in the methane reforming reaction, Ce-doped Ni-based catalysts demonstrate enhanced resistance to carbon deposits and exhibit higher catalytic activity. This improvement is attributed to the electron modification of Ni active sites by Ce, as well as the enhanced adsorption of reactants. The optimization of desorption behavior allows the reaction to proceed under milder conditions, thereby effectively improving both reaction efficiency and catalyst stability.[10–13] Cheng et al. utilized Ce-doped $Ni(OH)_2$/Ni-MOF nanosheets as efficient catalysts for oxygen evolution reactions, revealing excellent catalytic performance.[14] Concurrently, the La-doped Co_3O_4 catalyst showcases remarkable low-temperature activity in oxidation reactions.

By altering the concentration of surface oxygen species and the mobility of lattice oxygen within the catalyst, the activation energy of the reaction is reduced, which accelerates the reaction rate and enhances the purification of harmful gases.[15,16] Furthermore, the amount of rare earth element doping is critical for regulating catalyst performance. Variations in doping levels can lead to changes in the crystal structure, electron density, and surface properties of the catalyst, which subsequently affect the activity and selectivity of the catalytic reaction.[17] For example, adjusting the doping amount of Fe^{2+} can significantly enhance the electron conductivity of NiFe oxide, promoting the oxidation reaction of urea.[18] Rare earth element doping provides an effective means to enhance the catalytic performance of TiO_2. Due to their unique electronic structure, rare earth elements possess f-orbital electrons that can interact with the TiO_2 lattice, thereby modulating both the electronic and surface chemical properties of the catalyst.[19–23] By doping with rare earth elements, additional active sites can be introduced, optimizing the adsorption and activation processes of reactants, which in turn improves catalytic activity and selectivity.[24–26] Furthermore, the preparation of black TiO_2 typically involves the creation of oxygen vacancies, which can enhance electron transfer capacity and further boost catalytic activity. The support material for the catalyst significantly influences its activity, selectivity, and stability. Lanthanum (La) or Cerium (Ce) doped black TiO_2 is expected to exhibit exceptional properties in the glycerol selective oxidation reaction. On one hand, rare earth element doping can enhance the redox performance of the catalyst, leading to improved catalytic activity and selectivity during thermal catalysis. On the other hand, the presence of oxygen vacancies in black titanium dioxide facilitates better interaction between the reactants and the catalyst, thereby promoting the reaction progress.[27–30]

This study aims to investigate the performance of La and Ce doped black TiO_2 in the thermal catalytic reaction of glycerol oxidation. By examining the types and doping ratios of the doped elements, the catalyst exhibiting the best performance is identified. Characterization techniques such as XRD and XPS are employed to study the intrinsic relationship between catalyst structure and performance, thereby elucidating the catalytic action mechanism. The findings of this study provide an experimental foundation for the development of highly efficient alkali-free thermal catalytic materials for thermal oxidation reactions. Furthermore, it promotes advancements in biomass conversion and offers new insights into the application of rare earth element doped oxide catalysts in thermal catalytic reactions.

2. Materials and Methods

Tetrabutyl titanate ($C_{16}H_{36}O_4Ti$, A.R) from Shanghai Lin'en Technology Development Co., Ltd.; Glycerol (C_3H_8O, A.R) from Tianjin Fengchuan Chemical Reagent Technology Co., Ltd.; 3wt% Hydrofluoric acid (HF, A.R) from Shanghai Adamas Reagent Co., Ltd.; Absolute ethanol (C_2H_6O, A.R) from Tianjin New Technology Industrial Park Kemao Chemical Reagent Co., Ltd.; Potassium chloroplatinate (K_2PtCl_6, 99.95%) from Shanghai Adamas Reagent Co., Ltd.; Sodium borohydride ($NaBH_4$, 99.8%) from Shanghai Adamas Reagent Co., Ltd.; Cerium nitrate ($Ce(NO_3)_3{\cdot}6H_2O$, A.R) from Shanghai Adamas Reagent Co., Ltd.; Lanthanum nitrate ($La(NO_3)_3{\cdot}6H_2O$, A.R) from Shanghai Adamas Reagent Co., Ltd.

3. Results

3.1. Characterization of the Materials

Figure 1 present the X-ray diffraction (XRD) diagrams of La-B-TiO_2(Figure 1a) and Ce-B-TiO_2(Figure 1b), respectively, illustrating the effects of varying doping quantities. The characteristic TiO_2 peaks were observed at 25.3°, 37.8°, 48.0°, 53.9°, and 55.1°, corresponding to the anatase titanium dioxide (TiO_2) crystal planes (101), (004), (200), (105), and (211). Notably, the peak positions for TiO_2 in La-B-TiO_2 and Ce-B-TiO_2 remain unchanged, suggesting that the doping of La and Ce does not alter the TiO_2 structure, thereby confirming the successful incorporation of La and Ce. In Figure 1(a), the characteristic peaks for LaF_3 were recorded at 24.1°, 27.6°, 34.9°, and 43.7°. In Figure 1(b), the

Preprints.org (www.preprints.org) | NOT PEER-REVIEWED | Posted: 24 February 2025 doi:10.20944/preprints202502.1812.v1

characteristic peaks for CeF_3 appeared at 24.4°, 27.9°, 44.1°, and 45.2°. The presence of LaF_3 and CeF_3 can be attributed to the use of HF during the synthesis of RE-B-TiO_2, which resulted in the formation of trace amounts of LaF_3 and CeF_3 in the doped samples.

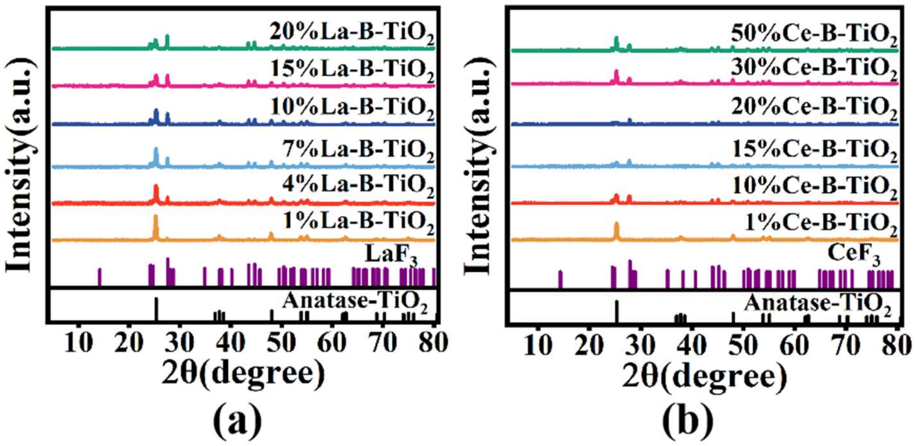

Figure 1. XRD patterns of (a) Ce-B-TiO_2 and (b) La-B-TiO_2 with different doping levels.

Figure 2 and Figure 3 illustrate the SEM images and mapping graphs for Pt/4%La -B-TiO_2 and Pt/30%Ce-B-TiO_2, respectively. The Pt/4%La-B-TiO_2(Figure 2a) and Pt/30%Ce-B-TiO_2(Figure 3a) supports exhibit a skeletal-like distribution, characterized by a high surface area ratio. Figure 2e reveals the distribution of Pt particles on the La-B-TiO_2, demonstrating that the Pt particles are uniformly distributed across the surface. In contrast, the La elements depicted in Figure 2d are sparse and scattered, which may account for the observed lower load capacity. For the Pt/30%Ce-B-TiO_2 catalyst, Figure 3e shows a uniform distribution of Pt particles. Figure 3d illustrates the uniform distribution of Ce elements. Furthermore, the results of the characterization indicate that the doping of Ce is substantial, which aligns with the experimental fact.

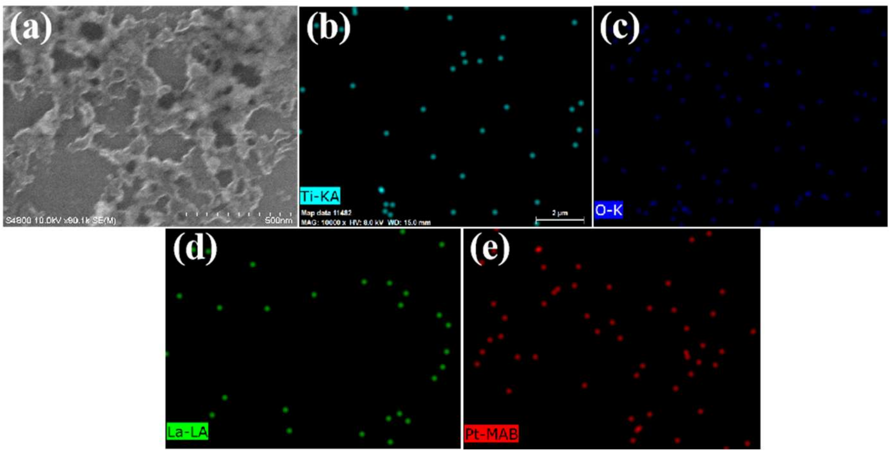

Figure 2. SEM-Mapping of Pt/La-B-TiO_2.

 doi:10.20944/preprints202502.1812.v1

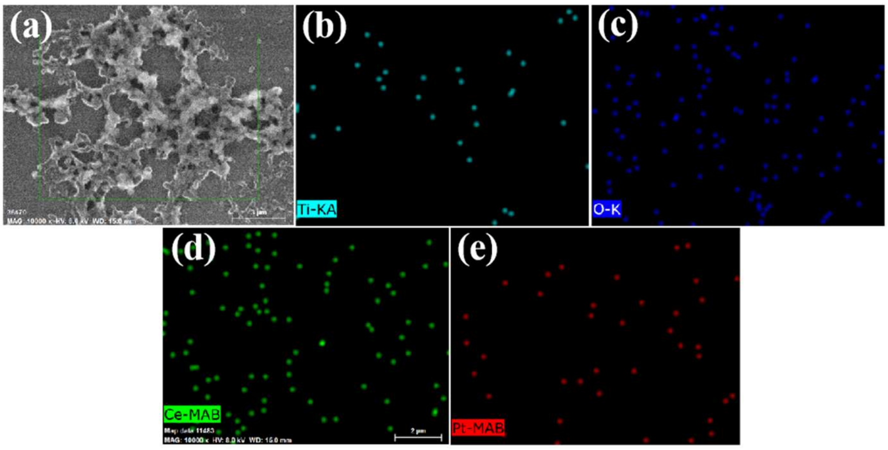

Figure 3. SEM-Mapping of Pt/Ce-B-TiO_2.

3.2. Selective Oxidation Reaction of Glycerol

The activity of the catalyst was evaluated through the glycerol oxidation reaction. Table S1 presents the activity data for the undoped catalyst. Conversion data collected over a period of 6 hours indicated that the catalyst exhibited the highest conversion when the reduction temperature of B-TiO_2 was set to 700°C. For subsequent doping experiments, Pt/B-TiO_2 (700°C) served as the base material, while the carrier B-TiO_2 (700°C) was doped with rare earth elements, specifically La and Ce.

Figure 4a illustrates the variation in the catalytic conversion rate of the Pt/Ce-B-TiO_2 catalyst over time at different doping ratios of Ce. During the initial two hours of the reaction, the conversion rates for catalysts with Ce doping ratios of 1%, 10%, and 15% were low. In contrast, the catalytic activity for the 20% doping ratio was moderate, while the Pt/30%Ce-B-TiO_2 and Pt/50%Ce-B-TiO_2 catalysts exhibited high catalytic activity. After two hours, the conversion rate reached 40%. By the 6h, the conversion rates for Pt/30%Ce-B-TiO_2 and Pt/50%Ce-B-TiO_2 were 87.10% and 77.82%, respectively (see Table S1). Figure 4b illustrates the selectivity changes of the Pt/Ce-B-TiO_2 catalyst for glyceric acid over time at various doping ratios. The data indicate that the selectivity for glyceric acid remains consistent across all six doping ratios, with an increasing trend over time. Notably, the catalysts Pt/30%Ce-B-TiO_2 and Pt/50%Ce-B-TiO_2 exhibited particularly strong performance. After 4 hours of reaction, Pt/50%Ce-B-TiO_2 achieved the highest selectivity for glyceric acid at 62%. However, at this point, its conversion rate (77.82%) was lower than that of Pt/30%Ce-B-TiO_2 (87.10%). From a yield perspective (see Figure 4d), the activity of catalysts can be assessed after 6 hours, with Pt/30%Ce-B-TiO_2 achieving the highest yield at 52.87%. The catalytic data presented in Table S1 demonstrate that the activity and selectivity for glyceric acid are enhanced in the doped catalysts compared to the undoped Pt/B-TiO_2 (700°C). Over the 6-hour reaction period, Pt/30%Ce-B-TiO_2 exhibited a 20% increase in conversion rate and a 25% increase in glyceric acid selectivity compared to Pt/B-TiO_2. In summary, the catalyst Pt/30%Ce-B-TiO_2 displays the highest catalytic performance.

 doi:10.20944/preprints202502.1812.v1

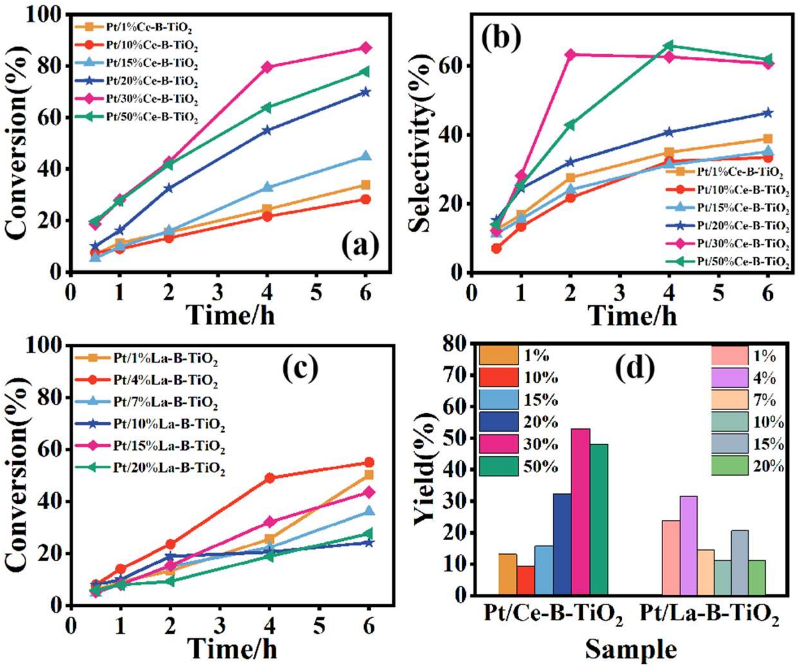

Figure 4. The conversion (a) and the selectivity (b) of Pt/Ce-B-TiO_2 with different Ce doping ratios, the conversion of Pt/La-B-TiO_2 (c) with different La doping ratios. The yield of Pt/Ce-B-TiO_2 and Pt/La-B-TiO_2 with different Ce or La doping ratios.

Figure 4c illustrates the variation in catalytic activity across different doping ratios of La in the Pt/La-B-TiO_2 catalyst, with the La doping amount controlled between 1% and 20%. In comparison to the catalytic activity of the Pt/La-B-TiO_2 catalyst depicted in Figure 4a, the overall catalytic activity of the Pt/La-B-TiO_2 catalyst is relatively low. Notably, Pt/4%La-B-TiO_2 exhibited the highest catalytic activity after 6 hours, achieving a value of 55.05%. However, when compared to the catalytic activity of the undoped Pt/B-TiO_2 at 700°C, the catalytic activity of Pt/4%La-B-TiO_2 did not show a significant improvement. This suggests that the doping of La has a limited effect on the activity of the Pt/B-TiO_2 structural catalyst. Figure S1 illustrates the change in glyceric acid selectivity of the Pt/La-B-TiO_2 catalyst over time, while Table S1 presents the data for selectivity of glyceric acid by Pt/La-B-TiO_2 after 6h. The observed trends and data indicate that the doping of La has a significant regulatory effect on the selectivity of the Pt/B-TiO_2 catalyst. As the amount of La doping increases, there is a discernible trend towards enhanced selectivity for glyceric acid in the Pt/La-B-TiO_2 catalyst. The experimental data suggest that the optimal doping ratio is 4%. Furthermore, when considering the conversion data, it is evident that the yield of Pt/4%La-B-TiO_2 after 6 hours of reaction is 31.86%. This represents an improvement in yield compared to the undoped Pt/B-TiO_2 (700°C).

4. Discussion

To investigate the influence of the doping amounts of La and Ce on the catalysts structure of Pt/La-B-TiO_2 and Pt/Ce-B-TiO_2, as well as the impact of catalyst structure on catalytic performance, we conducted X-ray photoelectron spectroscopy (XPS) analysis. This analysis focused on the valence state and content of Pt and Ti in three catalysts: Pt/30%Ce-B-TiO_2, Pt/50%Ce-B-TiO_2, and Pt/4%La-B-TiO_2 (Figure 5). The result indicate that the 4f spectrum of Pt in these catalysts comprises six peaks (Figure 5a-5c), which correspond to three valence states: Pt^0, Pt^{2+}, and Pt^{4+}. The Ti2p spectrum reveals four peaks (Figure 5d-5f), with peaks at 458 eV and 464 eV attributed to Ti^{3+}, while peaks at 459 eV and 465 eV correspond to Ti^{4+}. The peak position data and content information for Pt^0 and Ti^{3+} are summarized in Table S2. The doping of La and Ce has significant effect on the valence state and content of Pt in the catalyst. The content of Pt^0 in the catalyst Pt/La-B-TiO_2 (Figure 5c) was higher than that in the catalyst Pt/Ce-B-TiO_2 (Figure 5a-5b), with the Pt/30%Ce-B-TiO_2 exhibiting the highest Pt^0

 doi:10.20944/preprints202502.1812.v1

content. In the selective oxidation reaction of glycerol, the catalyst Pt/30%Ce-B-TiO_2 demonstrated the highest yield of glyceric acid, indicating that Pt^0 plays a crucial role in the catalytic reaction.

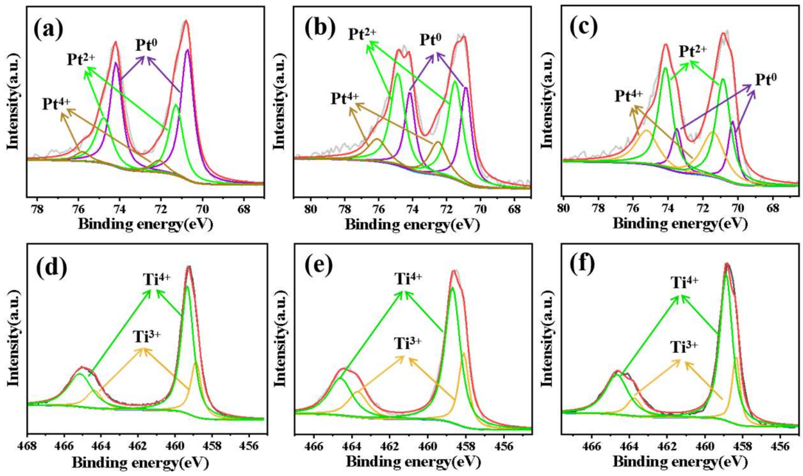

Figure 5. The XPS spectra of Pt 4f and Ti 2p in Pt/30%Ce-B-TiO_2(a and d), Pt/50%Ce-B-TiO_2(b and e) and Pt/4%La-B-TiO_2(c and f).

The Ti^{3+} content in the catalyst is calculated based on the ratio of Ti^{3+} to the sum of Ti^{3+} and Ti^{4+}. The data presented in Table S2 indicates that Ti^{3+} constitutes 22.51% in Pt/4%La-B-TiO_2, 26.60% in Pt/30%Ce-B-TiO_2, and 30.06% in Pt/50%Ce-B-TiO_2. This suggests that the doping of La and Ce does not significantly affect the Ti^{3+} content in the catalyst support. However, the amount of Ce in the Pt/Ce-B-TiO_2 catalysts have a notable impact on the Ti^{3+} content, as evidenced by the observed data trends. Specifically, with an increase in Ce doping within the catalyst, the Ti^{3+} content also rises. Among the catalysts analyzed, Ti^{3+} represents the highest proportion in Pt/50%Ce-B-TiO_2. Since the concentration of Ti^{3+} directly influences the concentration of oxygen vacancies in the catalyst support, it is essential to examine the oxygen vacancies concentration within the catalyst.

Figure 6 shows the deconvoluted XPS spectrum for O 1s in Pt/30%Ce-B-TiO_2(Figure 6a), Pt/50%Ce-B-TiO_2(Figure 6b) and Pt/4%La-B-TiO_2(Figure 6c). The main peak at 530.0 eV is assigned to Ti^{4+}-O bond in TiO_2 lattice and it agreed well with the literature [31,32]. The peak observed at a binding energy of 531.0eV is attributed to the oxygen vacancy resulting from the presence of Ti^{3+} defects, with the area under the curve indicating the concentration of oxygen vacancies. Compared to La-B-TiO_2, Ce-B-TiO_2 exhibits a higher concentration of oxygen vacancies. Furthermore, a comparison of the oxygen vacancy concentrations in Pt/30%Ce-B-TiO_2 and Pt/50%Ce-B-TiO_2 reveals that the concentration of oxygen vacancies increases with higher levels of Ce doping, which correlates with the trend observed in Ti^{3+} content as shown in Figure 5.

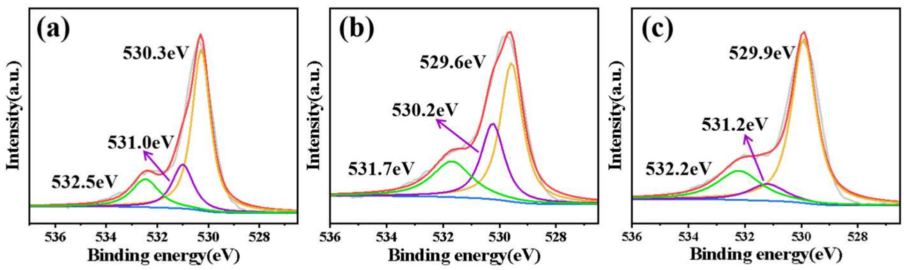

Figure 6. The XPS spectra of Pt 4f and Ti 2p in Pt/30%Ce-B-TiO_2(a and d), Pt/50%Ce-B-TiO_2(b and e) and Pt/4%La-B-TiO_2(c and f).

5. Conclusions

Based on the data analysis, the catalytic performance of the catalyst Pt/30%Ce-B-TiO_2 exhibits the highest catalytic activity over a duration of 6 hours, primarily attributed to the highest content of Pt^0. In the initial 4 hours, the catalytic activity of Pt/50%Ce-B-TiO_2 is comparable to that of Pt/30%Ce-B-TiO_2, likely due to the higher concentration of oxygen vacancies in Pt/50%Ce-B-TiO_2. However, as the reaction progresses, the concentration of oxygen vacancies in the catalyst support diminishes and the content of Pt0 also declines, resulting in lower catalytic activity compared to Pt/30%Ce-B-TiO_2 at 6h. Nevertheless, the selectivity for glyceric acid remains similar to that of Pt/30%Ce-B-TiO_2, approximately 60%. These experimental observations indicate that both the content of Pt^0 and the concentration of oxygen vacancies collectively influence the catalytic activity. Furthermore, the selectivity data presented in Table S2 reveal that the selectivity for glyceric acid is predominantly determined by the type of doping elements used. When the catalytic conversion rates are comparable, the selectivity of Pt/La-B-TiO_2 for glyceric acid demonstrates greater stability.

Supplementary Materials: The following supporting information can be downloaded at the website of this paper posted on Preprints.org.

Author Contributions: Conceptualization, X.Z. and L.D.; methodology, validation, formal analysis, Z.W. and X.Z.; investigation, Z.W. and X.Z.; resources, data curation, Z.W.; writing—original draft preparation, writing—review and editing, Z.W. and X.Z. and B.H. and H.Z.; visualization, Z.W. and X.Z.; supervision, L.D.; project administration, X.Z. and L.D.; funding acquisition, X.Z. and L.D.; All authors have read and agreed to the published version of the manuscript.

Funding: This research was supported by several funding sources, including the Inner Mongolia Autonomous Region Natural Science Foundation (2021BS02012), the Inner Mongolia Autonomous Region Higher Education Research Project (NJZY17455), and the Inner Mongolia Agricultural University High-level Talent Plan (NDYB2020-9), Key Laboratory of the Development and Resource Utilization of Biological Pesticide in Inner Mongolia.

Data Availability Statement: The data are available by directly contacting the author (lxyzxq@imau.edu.cn).

Acknowledgments: This work was supported by the Natural Science Foundation of Inner Mongolia Autonomous Region and the Inner Mongolia Department of Science and Technology.

Conflicts of Interest: The authors declare that the research was conducted in the absence of any commercial or financial relationships that could be construed as a potential conflict of interest.

References

1. Dasari, M.A.; Kiatsimkul, P.-P.; Sutterlin, W.R.; Suppes, G.J. Low-Pressure Hydrogenolysis of Glycerol to Propylene Glycol. *Appl. Catal. Gen.* **2005**, *281*, 225–231, doi:10.1016/j.apcata.2004.11.033.
2. Anitha, M.; Kamarudin, S.K.; Kofli, N.T. The Potential of Glycerol as a Value-Added Commodity. *Chem. Eng. J.* **2016**, *295*, 119–130, doi:10.1016/j.cej.2016.03.012.
3. Hu, X.; Lu, J.; Liu, Y.; Chen, L.; Zhang, X.; Wang, H. Sustainable Catalytic Oxidation of Glycerol: A Review. *Environ. Chem. Lett.* **2023**, *21*, 2825–2861, doi:10.1007/s10311-023-01608-z.
4. Dodekatos, G.; Schünemann, S.; Tüysüz, H. Recent Advances in Thermo-, Photo-, and Electrocatalytic Glycerol Oxidation. *ACS Catal.* **2018**, *8*, 6301–6333, doi:10.1021/acscatal.8b01317.
5. Katryniok, B.; Kimura, H.; Skrzyńska, E.; Girardon, J.-S.; Fongarland, P.; Capron, M.; Ducoulombier, R.; Mimura, N.; Paul, S.; Dumeignil, F. Selective Catalytic Oxidation of Glycerol: Perspectives for High Value Chemicals. *Green Chem.* **2011**, *13*, 1960, doi:10.1039/c1gc15320j.
6. Fujishima, A.; Zhang, X.; Tryk, D. TiO_2 Photocatalysis and Related Surface Phenomena. *Surf. Sci. Rep.* **2008**, *63*, 515–582, doi:10.1016/j.surfrep.2008.10.001.
7. Verma, V.; Singh, S.V. La-Doped TiO_2 Nanoparticles for Photocatalysis: Synthesis, Activity in Terms of Degradation of Methylene Blue Dye and Regeneration of Used Nanoparticles. *Arab. J. Sci. Eng.* **2023**, *48*, 16431–16443, doi:10.1007/s13369-023-08325-3.

8. Gong, Z.; Li, X.; Zhang, Z.; Liu, Y.; Song, H.; Wang, Y. Anodic Oxidation of TC4 Substrate to Synthesize Ce-Doped TiO_2 Nanotube Arrays with Enhanced Photocatalytic Performance. *J. Electron. Mater.* **2021**, *50*, 3276–3282, doi:10.1007/s11664-021-08821-y.
9. Kim, S.; An, E.; Oh, I.; Hwang, J.B.; Seo, S.; Jung, Y.; Park, J.-C.; Choi, H.; Choi, C.H.; Lee, S. CeO_2 Nanoarray Decorated Ce-Doped ZnO Nanowire Photoanode for Efficient Hydrogen Production with Glycerol as a Sacrificial Agent. *Catal. Sci. Technol.* **2022**, *12*, 5517–5523, doi:10.1039/D2CY00558A.
10. Liu, Y.; Gu, T.; Bu, C.; Liu, D.; Piao, G. Investigation on the Activity of Ni Doped Ce0.8Zr0.2O2 for Solar Thermochemical Water Splitting Combined with Partial Oxidation of Methane. *Int. J. Hydrog. Energy* **2024**, *62*, 1077–1088, doi:10.1016/j.ijhydene.2024.03.124.
11. Yang, Z.; Cui, Y.; Ge, P.; Chen, M.; Xu, L. CO2 Methanation over Rare Earth Doped Ni-Based Mesoporous Ce0.8Zr0.2O2 with Enhanced Low-Temperature Activity. *Catalysts* **2021**, *11*, 463, doi:10.3390/catal11040463.
12. Lincheng, X.; Yue, W.; Yong, Y.; Zhanzhong, H.; Xin, C.; Fan, L. Optimisation of the Electronic Structure by Rare Earth Doping to Enhance the Bifunctional Catalytic Activity of Perovskites. *Appl. Energy* **2023**, *339*, 120931, doi:10.1016/j.apenergy.2023.120931.
13. Dewoolkar, K.D.; Vaidya, P.D. Tailored Ce- and Zr-Doped Ni/Hydrotalcite Materials for Superior Sorption-Enhanced Steam Methane Reforming. *Int. J. Hydrog. Energy* **2017**, *42*, 21762–21774, doi:10.1016/j.ijhydene.2017.06.235.
14. Cheng, Y.; Zhu, L.; Gong, Y. Ce Doped Ni(OH)2/Ni-MOF Nanosheets as an Efficient Oxygen Evolution and Urea Oxidation Reactions Electrocatalyst. *Int. J. Hydrog. Energy* **2024**, *58*, 416–425, doi:10.1016/j.ijhydene.2024.01.208.
15. Duan, E.; Wang, Y.; Wang, S.; Bai, J.; Li, D.; Zhang, L.; Deng, J.; Tang, X. Revealing La Doping Activation or Inhibition of Crystal Facet Effects in Co3O4 for Catalytic Combustion and Water Resistance Improvement. *Chem. Eng. J.* **2024**, *496*, 153839, doi:10.1016/j.cej.2024.153839.
16. Bae, J.; Shin, D.; Jeong, H.; Kim, B.-S.; Han, J.W.; Lee, H. Highly Water-Resistant La-Doped Co_3O_4 Catalyst for CO Oxidation. *ACS Catal.* **2019**, *9*, 10093–10100, doi:10.1021/acscatal.9b02920.
17. Wang, Y.; Li, S.; Song, J.; Qu, H.; Yu, S. High-Pressure Hydrothermal Dope Ce into MoVTeNbOx for One-Step Oxidation of Propylene to Acrylic Acid. *Catal. Commun.* **2024**, *187*, 106849, doi:10.1016/j.catcom.2024.106849.
18. Li, Q.; Yuan, G.; Pan, T.; Wang, Y.; Xu, Y.; Pang, H. Design of Fe-Doped Ni-Based Bimetallic Oxide Hierarchical Assemblies Boost Urea Oxidation Reaction. *Int. J. Hydrog. Energy* **2024**, *93*, 338–345, doi:10.1016/j.ijhydene.2024.10.430.
19. Xie, K.; Jia, Q.; Wang, Y.; Zhang, W.; Xu, J. The Electronic Structure and Optical Properties of Anatase TiO_2 with Rare Earth Metal Dopants from First-Principles Calculations. *Materials* **2018**, *11*, 179, doi:10.3390/ma11020179.
20. Wakhare, S.Y.; Deshpande, M.D. Rare Earth Metal Element Doped G-GaN Monolayer : Study of Structural, Electronic, Magnetic, and Optical Properties by First-Principle Calculations. *Phys. B Condens. Matter* **2022**, *647*, 414367, doi:10.1016/j.physb.2022.414367.
21. Ducut, M.R.D.; Rojas, K.I.M.; Bautista, R.V.; Arboleda, N.B. Structural, Electronic, and Optical Properties of Copper Doped Monolayer Molybdenum Disulfide: A Density Functional Theory Study. *Mater. Sci. Semicond. Process.* **2025**, *185*, 108971, doi:10.1016/j.mssp.2024.108971.
22. Zhong, J.; Xu, Z.; Lu, J.; Li, Y.Y. Precise Electronic Structures of Amorphous Solids: Unraveling the Color Origin and Photocatalysis of Black Titania.
23. Naik, K.M.; Hamada, T.; Higuchi, E.; Inoue, H. Defect-Rich Black Titanium Dioxide Nanosheet-Supported Palladium Nanoparticle Electrocatalyst for Oxygen Reduction and Glycerol Oxidation Reactions in Alkaline Medium. *ACS Appl. Energy Mater.* **2021**, *4*, 12391–12402, doi:10.1021/acsaem.1c02195.
24. Zheng, B.; Fan, J.; Chen, B.; Qin, X.; Wang, J.; Wang, F.; Deng, R.; Liu, X. Rare-Earth Doping in Nanostructured Inorganic Materials. *Chem. Rev.* **2022**, *122*, 5519–5603, doi:10.1021/acs.chemrev.1c00644.
25. Zhao, Q.; Tian, X.; Ren, L.; Su, Y.; Su, Q. Understanding of Lanthanide-Doped Core–Shell Structure at the Nanoscale Level. *Nanomaterials* **2024**, *14*, 1063, doi:10.3390/nano14121063.
26. Bian, T.; Zhou, T.; Zhang, Y. Preparation and Applications of Rare-Earth-Doped Ferroelectric Oxides. *Energies* **2022**, *15*, 8442, doi:10.3390/en15228442.
27. Dinamarca, R.; Garcia, X.; Jimenez, R.; Fierro, J.L.G.; Pecchi, G. Effect of A-Site Deficiency in LaMn0.9Co0.1O3 Perovskites on Their Catalytic Performance for Soot Combustion. *Mater. Res. Bull.* **2016**, *81*, 134–141, doi:10.1016/j.materresbull.2016.05.007.

doi:10.20944/preprints202502.1812.v1

28. Li, G.; Li, X.; Hao, X.; Li, Q.; Zhang, M.; Jia, H. Ti3+/Ti4+ and Co2+/Co3+ Redox Couples in Ce-Doped Co-Ce/TiO2 for Enhancing Photothermocatalytic Toluene Oxidation. *J. Environ. Sci.* **2025**, *149*, 164–176, doi:10.1016/j.jes.2023.10.025.
29. Nain, P.; Pawar, M.; Rani, S.; Sharma, B.; Kumar, S.; Majeed Khan, M.A. (Ce, Nd) Co-Doped TiO2 NPs via Hydrothermal Route:Structural, Optical, Photocatalytic and Thermal Behavior. *Mater. Sci. Eng. B* **2024**, *309*, 117648, doi:10.1016/j.mseb.2024.117648.
30. Li, Z.; Wang, E.; Zhang, Y.; Luo, R.; Gai, Y.; Ouyang, H.; Deng, Y.; Zhou, X.; Li, Z.; Feng, H. Antibacterial Ability of Black Titania in Dark: Via Oxygen Vacancies Mediated Electron Transfer. *Nano Today* **2023**, *50*, 101826, doi:10.1016/j.nantod.2023.101826.
31. Panda, A.B.; Mahapatra, S.K.; Barhai, P.K.; Das, A.K.; Banerjee, I. Understanding of Gas Phase Deposition of Reactive Magnetron Sputtered TiO2 Thin Films and Its Correlation with Bactericidal Efficiency. *Appl. Surf. Sci.* **2012**, *258*, 9824–9831, doi:10.1016/j.apsusc.2012.06.037.
32. Abdullah, S.A.; Sahdan, M.Z.; Nafarizal, N.; Saim, H.; Embong, Z.; Cik Rohaida, C.H.; Adriyanto, F. Influence of Substrate Annealing on Inducing Ti3+ and Oxygen Vacancy in TiO2 Thin Films Deposited via RF Magnetron Sputtering. *Appl. Surf. Sci.* **2018**, *462*, 575–582, doi:10.1016/j.apsusc.2018.08.137.